


SCIENTIFIC REPORTS



OPEN

Strong improvement of the transport characteristics of $\text{YBa}_2\text{Cu}_3\text{O}_{7-x}$ grain boundaries using ionic liquid gating

A. Fête & C. Senatore 

For more than 30 years, the remarkable superconducting properties of $\text{REBa}_2\text{Cu}_3\text{O}_{7-x}$ (RE = rare earth) compounds have triggered research studies across the world. Accordingly, significant progresses have been made both from a basic understanding and a fabrication processes perspective. Yet, today, the major technological bottleneck towards the spread of their practical uses remains the exponential decay of their critical current with grain misorientation in polycrystalline samples. In this work, we used an ionic liquid to apply extremely high transverse electric fields to $\text{YBa}_2\text{Cu}_3\text{O}_{7-x}$ thin films containing a single well-defined low-angle grain boundary. Our study shows that this technique is very effective to tune the IV characteristics of these weak-links. In-magnetic field measurements allow us to discuss the type of the vortices present at the grain boundary and to unveil a large variation of the local depairing current density with gating. Comparing our results with the ones obtained on chemically-doped grain boundaries, we discuss routes to evaluate the role of local strain in the loss of transparency at cuprates low-angle grain boundaries. In short, this study offers a new opportunity to discuss scenarios leading to the reduced transport capabilities of grain boundaries in cuprates.

A widely accepted fact in the high-temperature superconductors community is that the major bottleneck to the spread of practical uses of $\text{YBa}_2\text{Cu}_3\text{O}_{7-x}$ (YBCO) is the exponential decay of its critical current density (J_c) with grain misorientation angle (θ) in polycrystalline samples¹. For this reason, for more than 30 years, intense research efforts have been devoted to the study of cuprate grain boundaries (GBs). Nowadays, two main lines have emerged. The first one makes uses of grain boundaries to fabricate high quality Josephson junctions for SQUID applications^{2,3}. The second one minimizes the impact of GBs on the transport properties of YBCO based technical conductors by growing the cuprate layer on a highly textured tape by physical or chemical routes^{4,5}. Nowadays, the level of texturing of these coated conductors is impressive, reaching in-plane misalignments of just a few degrees over hundreds of meters⁶.

Conventionally tape texturing is achieved using one of two methods. The first one, Rolling-Assisted Biaxial Texturing (RABiTS)⁷, makes use of a series of deformations and recrystallizations to shape a polycrystalline Ni-alloy tape so that its cubic structure is oriented both in- and out-of- the tape plane. The second one, Ion Beam Assisted Deposition (IBAD)⁸, uses an Ar^+ beam at 45° incident angle relative to the tape surface during the deposition of an MgO buffer layer, in order to orient it in-plane. Both techniques require, in addition, a set of buffer layers to prevent diffusion between the layers and to fine tune the in-plane lattice parameter of the material in contact with the cuprate. These roads are complex and hence it is still nowadays a technological challenge to achieve the required tape perfection over 1 km, which is the typical length for applications.

For this reason, investigations aiming at understanding the physical mechanisms limiting the current through cuprate GBs and on techniques able to rise their transparency are highly relevant from a technological point of view. Actually, even low-angle grain boundaries ($\theta < 10^\circ$) are an important bottleneck for the development of the industry of superconductors as textured tapes cannot eliminate them completely. This is the reason why here we focus on a set of $\theta = 8^\circ$ YBCO GBs, as they represent a relevant technological problem and a reasonably degraded starting point in term of superconducting properties.

Department of Quantum Matter Physics (DQMP), University of Geneva, Geneva, Switzerland. Correspondence and requests for materials should be addressed to A.F. (email: alexandre.fete@unige.ch)

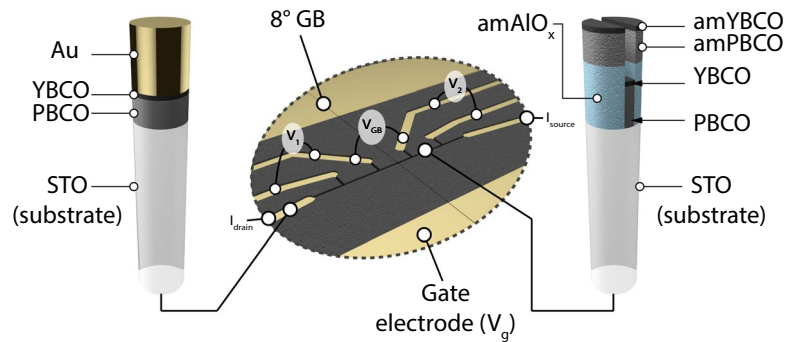


Figure 1. Channel layout and taps naming. The IL is not represented but covers the whole channel and the gate electrode. Core samples of different regions are drawn on the left and on the right of the figure (see Methods). An amorphous (am) layer of AlO_x is used to prevent the coherent growth of PBCO and YBCO on selected area, making these regions highly insulating¹¹.

On the theoretical side GBs are complicated objects. They combine the complex phase diagram of a relatively low carrier density material with charge and strain perturbations that evolve on nanometric lengthscales⁹. Due to the short coherence length (ξ) in these materials, these rapid variations impact the local order parameter and have profound implications on the vortex matter. For example, depending on the ratio between the local depairing current density in the bulk and at the grain boundaries, vortices of Abrikosov (A), Abrikosov-Josephson (AJ) or Josephson (J) type are created above the lower critical field ($B_{c,1}$)¹⁰. Ultimately the pinning force and the vortex dynamics are modified.

In a previous work¹¹, we demonstrated the effectiveness of ionic liquid (IL) gating to tune the transport properties of pulsed laser deposition (PLD) grown ultra-thin and single-crystalline YBCO films. More precisely, using the electric field produced by an ionic liquid biased by a gate voltage V_g , we were able to double the T_c and increase eightfold the critical current of underdoped YBCO films. The evolution of the critical parameters (J_c , T_c) was shown to be consistent with the existing literature on chemically doped YBCO films.

In this work, we applied the same technique to YBCO low angle grain boundaries obtained by growing epitaxially cuprate thin films on SrTiO_3 (STO) (001) bi-crystals. By applying a few volts between the liquid and the thin film, a large evolution of the critical parameters of the boundary was observed. Analyzing our results in the framework developed by Gurevich¹² allowed us to unveil a large evolution of the local depairing density at the GB ($J_{d,GB}$) upon doping. As mentioned above this quantity is key to determine the type of vortices at the weak-link and its tuning represents an opportunity since vortex pinning is intimately linked to the characteristics of the vortices. In addition to that, since IL gating does not *a priori* modify the stress level at the GB, we discuss a strategy to evaluate the relative importance of strain release in the large improvement of the GB transparency obtained following the well known Ca-doping route¹³.

Results

As mentioned in the introduction, our field effect devices use YBCO as superconducting layer and STO as substrate. Figure 1 clarifies the geometry that was used in this study. The channel is divided into three parts. GB-free regions are bounded by the electrical contacts of V_1 and V_2 while the part of the channel crossed by the 8° GB is measured using tap V_{GB} . We used this scheme to have a control over the contribution to V_{GB} of the region located before and after the GB in the central part of the device. Also, due to variations of the substrate quality and of the miscut angle between the two part of the bi-crystalline substrate, $T_{c,s}$ and $J_{c,s}$ recorded on V_1 and V_2 were not always equal. In what follows, we always refer to the worst of the two GB-free region when we write $V_{1,2}$. Indeed, this is the weak-link free region with the poorest superconducting properties that will first contribute to V_{GB} .

Not depicted on Fig. 1 is the IL which covers the whole channel and the gate. A difference of potential V_g , applied between the gate electrode and the grounded channel moves the ions in the liquid and leads to the creation of an electrical double layer (EDL) at the interface between the liquid and the YBCO film. This EDL is a region where a very quick drop of potential occurs which is equivalent to an extremely high electric field. As mentioned above, this electric field can be used to greatly tune the superconducting properties of ultra-thin YBCO films^{11,14–18}. More details on sample growth and on the IL can be found in the Methods.

Figure 2 shows the low temperature (4.2 K), self-field (sf), current-voltage (IV) characteristics of our YBCO films. 5, 7 and 10 unit cells (uc) thick samples are presented. V_g is defining the color code. Before developing further the analysis of the data, let us first clarify an important point.

As can be observed from the data defining the color code, our samples are underdoped, with an initial T_c of 18.7, 48.6 and 73.8 K, respectively for the 5, 7 and 10uc samples. T_c is evaluated at $R=0$. This situation is standard for ultrathin cuprate layers¹⁹ and is probably largely stemming from the lattice mismatch between the substrate and the film. As discussed in¹¹, the absence of a capping layer protecting the YBCO and the hygroscopic properties of ILs also play a role. It is noteworthy that we repeated the procedure presented in¹¹ and verified that the GB-free regions of the 5, 7 and 10uc samples of this study display an evolution of their T_c and J_c which is inline with the homogeneous doping of an underdoped YBCO film. These data are presented in the Supplementary information.

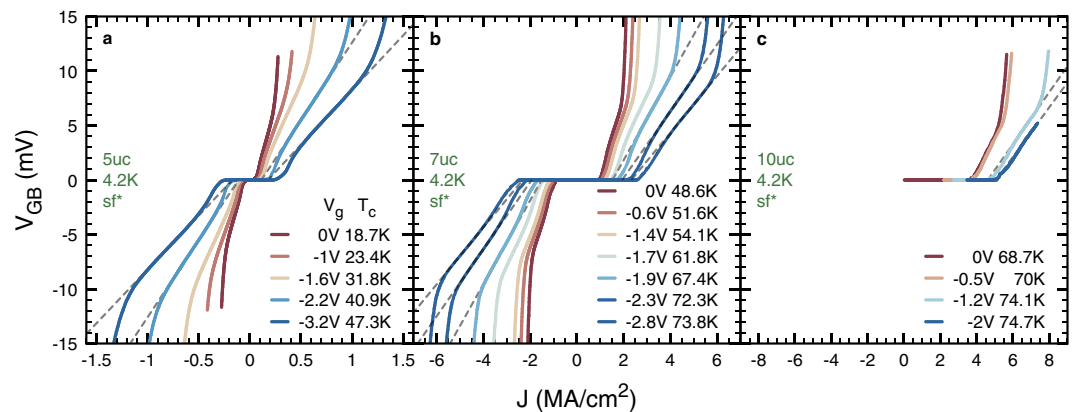


Figure 2. Gate tuned, low temperature, self-field, current-voltage characteristics of V_{GB} (see Fig. 1) for samples with 5 **a**, 7 **b** and 10uc **c** thick YBCO layer. Dashed lines highlight the high current linear behavior. For readability, they are not drawn for all V_g .

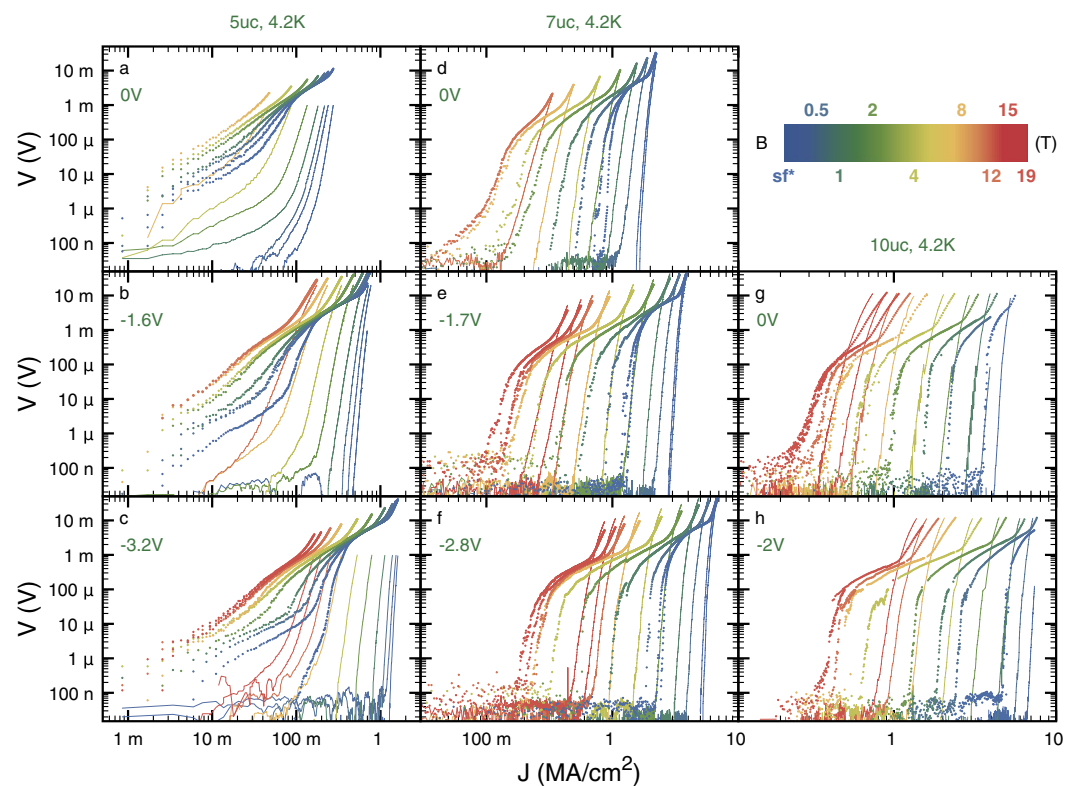


Figure 3. Gate tuned, low temperature, current-voltage characteristics of V_{GB} (points) and $V_{1,2}$ (lines) for increasing magnetic fields and for samples with 5 (**a-c**), 7 (**d-f**) and 10uc (**g** and **h**) thick YBCO layer. For readability, we present only the data at the minimum (**a,d,g**), average (**b** and **e**) and maximum (**c,f,h**) V_g . The minimum of the V axis is set to the $1\mu\text{V cm}^{-1}$ criterion.

Hence, through the use of 5, 7 and 10uc YBCO layers and IL gating, we present in Fig. 2, strong tunings of underdoped YBCO GBs, for various initial doping levels. Clearly, not only the critical current of the GB but also the overall shape of the IVs is tuned by V_g , pointing to a strong modification of the GB barrier properties.

In Fig. 3, we show a selection of the low temperature magnetic field dependence of our IVs, the latter being applied perpendicularly to the c -axis of the film. Together with the data acquired on V_{GB} (points), we present data recorded using taps $V_{1,2}$ (lines). Interestingly, at the highest currents, V_{GB} develops a strong non-linearity for all dopings and magnetic fields. Comparing with the IV curves of taps $V_{1,2}$, one infers that this non-linearity is to be attributed to the onset of dissipation in the superconducting electrodes of V_{GB} . Indeed, it develops only when $V_{1,2}$ starts dissipating. As a matter of consequence, at lower currents, V_{GB} is representative of the dissipative processes taking place at the GB. Hereafter, we use the term “superconducting electrodes” for the regions of the channel

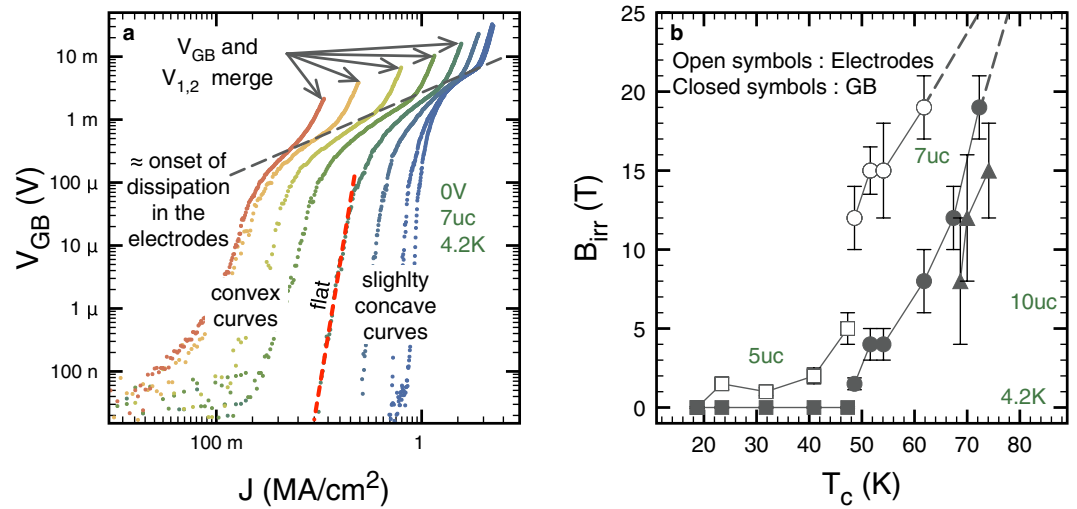


Figure 4. Tuning of the irreversibility field using IL gating. **(a)** Exemplary IV set (only V_{GB}) in order to illustrate the concepts discussed in the main text. At high currents, an upward curvature is observed that can be attributed to dissipation in the superconducting electrodes located in-between the taps of V_{GB} . At low current depending on the magnetic field, a log-flat or convex curvature can be observed in a log-log scale. The magnetic field at which the flattest IV curve is observed is used to estimate B_{irr} . **(b)** Evolution of B_{irr} with the T_c of the superconducting electrodes. Open symbols are for measurements obtained using $V_{1,2}$ and closed symbols are for measurements obtained using V_{GB} . B_{irr} has been computed averaging over the two current polarities and the error bars have been computed accordingly taking into account the large field steps used in our experiments. Dashed lines are linear extrapolations that highlight the fact that at the highest doping $B_{irr} > 19T$.

located before and after the GB and bounded by the contacts of V_{GB} . This non-linearity can also be observed in Fig. 2, above the ohmic-like regime highlighted on selected curves by a dashed line.

Another interesting point of the dataset presented in Fig. 3, is the fact that, at low currents, many of the IVs change curvature (slightly concave to convex) upon magnetic field increase and for many of the doping levels. This is true for both V_{GB} and $V_{1,2}$. This concept is illustrated for V_{GB} in Fig. 4a together with the ones pertaining to the discussion on the onset of dissipation in the superconducting electrodes. Following²⁰, we attribute this behavior to the melting of the vortex lattice. Indeed, though our data are quite scattered in this regime, at the lowest currents and above the “concave to convex” transition (*i.e.* on the left of the “flat” line in Fig. 4a) our IVs tend to a linear behavior which is characteristic of vortex free-flow. Hence we define the irreversibility field (B_{irr}) for both V_{GB} and $V_{1,2}$ as the magnetic field at which the change of curvature takes place. Using this criterion, we were able to highlight a strong tuning of the B_{irr} of the inter- and intra-grains channels with IL gating. Our results are summarized in Fig. 4b. The transition temperature of the superconducting electrodes is used as a scale to define the overall doping level of the system¹¹. When B_{irr} is high, large error bars are present due to the large field steps.

The evolution shown in Fig. 4b is large. For example, for the inter-grains data acquired on the 7uc sample at 4.2 K, B_{irr} moves from 1.5 T to unobservably high (*i.e.* $B_{irr} > 19T$). In addition to that, Fig. 4b spotlights a ~ 10 K T_c -shift, when one confronts the B_{irr} measured using V_{GB} and $V_{1,2}$. Remembering that T_c is representative of the superconducting electrodes and that it is just a convenient indicator of the average doping level of the system, this observation suggests that a GB needs a comparatively higher doping state to display the same B_{irr} as the grains. This observation is in line with the globally reduced T_c expected at cuprate grain boundaries.

The vortex dynamics along planar defects has been studied theoretically in an extensive manner by Gurevich during the 90’s^{10,12,21,22}. He found that vortices in grain and at grain boundaries, while sharing similarities, are different. In particular, conventional Abrikosov (A) vortices with normal core size defined by the coherence length ξ evolve to mixed Abrikosov-Josephson (AJ) vortices at low angle grain boundaries. Among other interesting properties, AJ vortices have an extended Josephson core along the GB whose size is increasing with the driving current density and the externally applied magnetic field. Hence upon current and magnetic field ramping AJ vortices can overlap. This property leads to the appearance of a magnetic field independent differential resistance at high enough current density, as observed for example in²⁰ and even to current driven transition from AJ to J-like vortices²³ in more weakly pinned systems. This contrasts sharply with A vortices that have current independent core size ξ and overlap only at the upper critical field ($B_{c,2}$).

This scenario describes the V_{GB} dataset of Fig. 3 very satisfactorily, at least qualitatively. At low currents, AJ vortices are present but depending on the value of the irreversibility field they are pinned or not by the GB. Unpinned AJ vortices lead to the appearance of a magnetic field dependent flux flow resistance R_f as can be observed, for example, on almost all the curves of the 5uc sample in Fig. 3. With increasing driving current, the size of the AJ vortices along the GB increases. For pinned vortices this lowers the associated pinning force and eventually leads to dissipation. At some point, the core of the AJ vortices is so large that AJ vortices overlap, generating a normal barrier with a resistance independent of the magnetic field.

Noteworthy, the presence of a magnetic field independent differential resistance on all the curves of Fig. 3 while the system is in a superconducting or vortex flow state at lower current disqualifies A vortices. Indeed, the constant size of A vortices implies that if a constant differential resistance is observed then $B > B_{c,2}$, but in this case the IV curve is predicted to be ohmic which is not the case here. Reversely, the large difference between the applied magnetic fields of this study and the $B_{c,1}$ expected in the YBCO system, *a fortiori* at YBCO GBs, exclude that non-overlapping Josephson vortices are present at low currents in our measurements. These considerations are coherent with the idea the AJ vortices are the driving force behind the shape of the IVs presented in Figs 2 and 3.

Quantitatively, the theory developed in^{12,24}, that describes the IVs generated by a single row of moving AJ vortices, predicts that $R_f = R_N \sqrt{\frac{B}{B+B_0}}$, with $B_0 = \frac{\phi_0}{(2\pi l)^2}$, ϕ_0 the quantum of flux, l the phase core length and R_N the excess GB quasi particle resistance. Unfortunately, it is clear from the scattering of our data, especially at low currents, that the extraction of reliable values for B_0 is not possible here. Indeed the quadratic relation between B_0 and the flow/normal state resistances plus the ability of moving vortices at GBs to drag neighboring vortices in the superconducting electrodes²⁵ require a careful treatment, with much finer current and magnetic field steps.

Nevertheless, it is reasonable to think that the evolution of the magnetic field-independent resistance observed just before the onset of dissipation in the electrodes is representative of the evolution of R_N , the excess GB quasi particle resistance. Indeed, at high currents, where AJ vortices overlap, the above-mentioned drag force of AJ vortices drops to zero²⁶. It remains that the determination of R_N from transport measurements alone is a difficult task. Hence, in what follows, we write the magnetic field independent resistance observed at high current in our measurements R_N^* and derive our conclusion mainly from its relative variation.

Another quantity of interest, in Gurevich's theory of the vortex dynamics along planar defects, is the depairing current density at the GB, $J_{d,GB}$. Indeed, in this framework, it can conveniently be estimated from the steepest slope of the GB IVs recorded at low magnetic fields. However, before going further and evaluating it from our data, we must consider the following.

First, Gurevich's model is postulating a spatially homogeneous weak-link, with a constant and low $J_{d,GB}$. According to the same author⁹, this is far from being true at YBCO grain boundaries especially in the underdoped regime where strain driven variation of T_c are emphasized. Secondly, as mentioned in the Methods, the lateral width of our bridges is 10 μm . Since this value is relatively large, care must be taken when evaluating $J_{d,GB}$ in the Meissner state because self-field effects can impact the uniformity of the current distribution. Thirdly, in low magnetic fields, magnetic geometrical barriers might be present and create current inhomogeneities as well.

It is clear from the above list of physical phenomena, that, strictly speaking, we should restrict ourself to a determination of a lower bound for $J_{d,GB}$. However, we are convinced that at least part of the physics raised in the last paragraph can be addressed by considering the details of our devices.

First, the dislocation network present at low-angle GBs, that reduces the cross-section available for transport by creating fully insulating regions, has been studied experimentally by Sarnelli²⁷. He found that for an 8° GB this reduction accounts for a factor ~ 2.9 . Hence, in what, follows, we rescaled $J_{d,GB}$ by this amount. Secondly, due to the ultra thin nature of our films, it is theoretically predicted that the correct magnetic penetration depth to consider here is the Pearl length, $\Lambda = 2\lambda^2/d$ with λ the London penetration depth and d the film thickness. It turns out that, in our case, Λ is of the order of the width of our bridges (or even larger if we consider the underdoped state of our devices). Hence, the current peaks typically observed in the Meissner state of long junctions should strongly overlap in our case, leading to a relatively homogeneous current distribution. In summary, it is reasonable to think that the extraction of $J_{d,GB}$ from our measurement, while not representing a fully quantitative determination of the real local depairing current density at the GB, deserves to be analyzed.

In Fig. 5, we focus on the self-field evolutions of the contact resistance R_N^*A and of $J_{d,GB}$ with T_c . $A = w \times t$ is the surface of the GB perpendicular to the current flow, with w the width of the channel and t the thickness of the film. Clearly, the tuning induced by IL gating is remarkable. R_N^* is reduced by 70, 60 and 30% for the 5, 7 and 10uc samples respectively. Concomitantly, $J_{d,GB}$ increases by 310, 170 and 40% respectively.

To get a point of comparison, we computed the expected depairing current density J_d for an underdoped YBCO bulk in the limit of low temperatures. From the Ginzburg-Landau (GL) theory, it can be shown that, close to T_c , $J_d = \sqrt{\frac{2\Phi_0}{27\pi\mu_0^2}} \sqrt{\frac{B_{c,2}}{\lambda^2}}$ with Φ_0 the magnetic flux quantum and μ_0 the vacuum permeability²⁸. Yet, GL theory is only valid close to T_c . Fortunately, it can be shown that the results from the Kupriyanov-Lukichev (KL) theory²⁹, valid at low temperature, can be recovered through a simple scaling factor. Namely, $J_d^{KL} \sim 0.35J_d^{GL}$ at $T/T_c \ll 1$. For $B_{c,2}$ we used the data from³⁰, and for λ the data from³¹.

Figure 5b shows that J_d is always several times $J_{d,GB}$. This corroborates the existence of AJ vortices in our system since their self-field length l along the GB can be estimated by $l \sim \xi J_d/J_{d,GB}$. Another interesting quantity is the ratio between $J_{d,GB}$ and the expected depairing current density in the virgin state of the system (minimum T_c of each series of data). In this case, one is interested to know if in a hypothetical bulk of a fixed T_c , the action of IL gating on the GB is able to bring $J_{d,GB}$ back to a sizable fraction of J_d . Figure 5c shows that this is indeed the case, especially for our thinnest film, which exhibits a complete restitution of our estimation of the local depairing current density at the GB. For the 7 and 10uc samples the effect is smaller. This can be explained, at least partially, by an increased volume to dope and by a higher initial doping level. It is also interesting to note that in the virgin state of our 8° GBs, $J_{d,GB}/J_d \sim 0.25$ independently of the initial doping level.

To conclude this section we would like to comment briefly on the discontinuity of $J_{d,GB}$ observed in Fig. 5b when we move from the 5uc sample to the 7uc sample. This contrasts sharply with the smooth evolutions obtained using IL gating and indicates that the state created by starting from an underdoped grain boundary and doping it to a given level of T_c can be different from a natively higher T_c state. In fact, this is not surprising if one

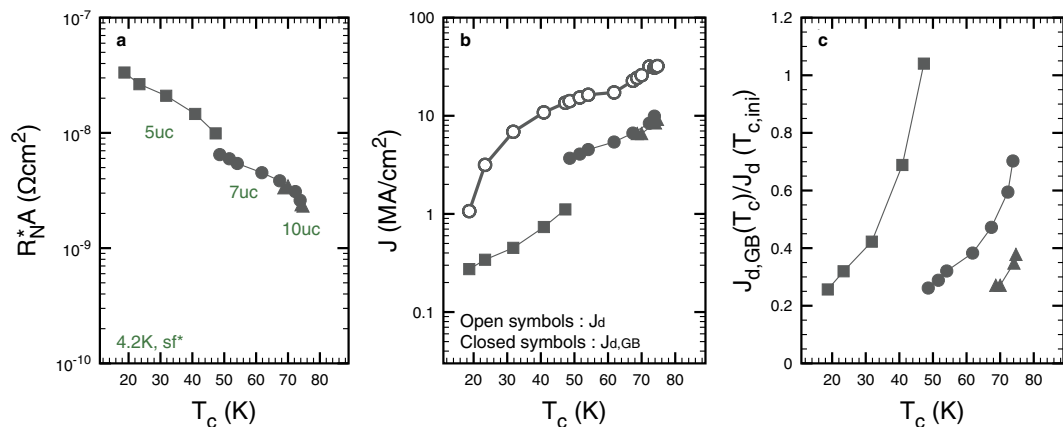


Figure 5. Evolution of the key parameters describing the gate induced improvements of our 5, 7 and 10uc weak-links. The transition temperature of the superconducting electrodes (T_c) is used as a scale to define the overall doping level of the system¹¹. The same convention linking the shape of the markers and the sample type is used for all the graphs. (a) Evolution of the contact resistance R_N^*A . (b) Evolution of the depairing current density at the GB ($J_{d,GB}$, closed symbols). These data are confronted with the depairing current density expected for a YBCO sample with no GB and of a given T_c (J_d , open symbols). (c) Evolution of $J_{d,GB}$ normalized by the value of J_d estimated in the state of lowest doping ($V_g = 0$ or $T_c = T_{c,ini}$).

remembers that T_c is representative of the superconducting electrodes. On its side, the GB has a distribution of critical temperatures⁹. This distribution can clearly be tuned by IL gating but most probably at a different pace than the superconducting electrodes.

Discussion

To date, the most successful method to improve the transport properties of YBCO GBs has been the partial substitution of Y^{3+} by Ca^{2+} in the cuprate lattice. For example, using this strategy, the 4.2 K self-field intergranular critical current of 24° [001]-tilt GBs was increased eightfold¹³. Similarly, the in-magnetic-field transport properties at 44 K of low angle GBs were strongly improved²⁰.

This approach is based on the fact that by partially substituting Y^{3+} by Ca^{2+} a strong overdoping of the cuprate structure is made possible. At the price of a global reduction of the film's T_c , this helps to recover the transport properties of GBs which are known to be carrier depleted. It is also established that Ca-doping reduces the deleterious strain fields extending from the GB dislocation cores. This is considered to be of special importance for very low angle GBs ($<5-7^\circ$)^{9,32}. Finally, Ca-doping has the advantage to increase the oxygen vacancy formation energy³³.

Importantly, transmission electron microscopy (TEM) investigations on low angle GBs showed that the intense electric and strain fields present at the GB induce a segregation of the Ca^{2+} cations to its tensile regions³⁴. This has the effect to expand the dislocation cores but leaves non-chemically doped channels in-between them, at least for low angle grain boundaries. As a matter of consequence, these nano-channels do not suffer from the T_c reduction induced by overdoping. Yet they maintain a quite high hole concentration due to the screening of the sheet GB charge density by Ca-doping. In³⁵, it was observed that in perpendicular fields and at relatively high temperatures these combined effects can lead to a relatively strong pinning and to an intergrain critical current exceeding the intragrain one.

Clearly, the chemical nature of Ca-doping makes it a quite complex technique to investigate cuprate GBs. While further investigations of the doping mechanism involved in IL gating are needed, it might well be simpler. For example, it is reasonable to think that the tuning presented in this paper is acting more homogeneously than Ca-doping. Indeed, along the GB, only fully insulating regions and regions displaying a very low quantum capacitance might be less tuned by our gating method³⁶. This contrasts sharply with the presence of Ca-doped, Ca-enriched and Ca-free regions in the Ca-doped samples. In addition to that, since no chemical substitution is involved in IL gating, the strain level at the GB can be considered as constant throughout our doping process. Finally, we do not expect an expansion of the dislocation cores with IL gating. Rather, depending on the initial carrier depletion profile along the GB, an expansion of the nano-channels can be envisaged.

Given these differences, it would be interesting to find a way to compare the degree of recovery that we achieved here in comparison with the Ca-doping road. Using the usual parametrization of T_c in cuprates $T_c/T_{c,max} = 1 - 82.6(p - 0.16)^{2.37}$, with $T_{c,max} = 93\text{K}$, we find that our gating experiments increase the number of hole per copper oxygen planes p by $\Delta p = 0.021, 0.026$ and 0.0075 respectively for the 5, 7 and 10uc samples. We stress here that this modulation is evaluated using the electrodes T_c , hence it should be interpreted as an average doping capability. In addition to that, the fact that Δp is larger for the 7uc than for the 5uc sample while the observed variations of R_N^* and $J_{d,GB}$ logically reduce with sample thickness informs us that Δp must be taken as indicative of an order of magnitude. Interestingly, as grown $Y_{0.7}Ca_{0.3}Ba_2Cu_3O_{7-x}$ films (*i.e.* with no *ex-situ* annealing) naturally display an overdoping of 10 to 20%^{13,32}. This corresponds to $\Delta p \sim 0.017 - 0.033$. Hence, IL gating seems to induce a carrier modulation that is comparable to the one achieved by Ca-doping.

The main difficulty in the parallel we try to draw is to find a point of comparison. Indeed, due to the very high critical currents densities admitted by low angle GBs far from T_c , we found only a few studies that we can compare with our data recorded at 4.2 K^{20,32}. Initially, we have been tempted to add to this list the seminal work by Schmehl *et al.* on 24° [001]-tilt GBs. Indeed, the underdoped state of our samples implies that the effect of charge depletion is possibly preponderant at our GBs. This is a distinctive feature of large angle GBs for which the strain decay length is much shorter than the Debye screening length (λ_D). In addition to that, experimentally, our self-field critical currents are similar to the ones obtained at standard ~30° YBCO GBs. However, the high magnetic fields sustained by our GBs clearly disqualify a Josephson junction scenario, the latter being known to apply at standard YBCO GBs with misorientation angles larger than ~15°. Hence, the electronic structure at the GBs of this study is probably very different to the one investigated in¹³.

If one focuses on the relative evolution of $J_{d,GB}$, we note that the tuning observed in self-field for the 5, 7 and 10uc samples of this paper is always larger or similar to the one that can be estimated for optimally Ca-doped low angle grain boundaries. We reached this conclusion using extrapolation of higher temperature data²⁰ and comparing with magneto-optical measurements³². We observed that, at best, the 4.2 K self-field J_c of low angle GBs is multiplied by a factor ~2 using Ca-doping. Using IL gating, we multiplied $J_{d,GB}$ by a factor 3.4, 2.7 and 1.9 for the 5, 7 and 10 uc respectively.

In summary, while acting *a priori* purely by increasing the charge density of the thin film, IL gating reaches a tuning of the GB critical current comparable to Ca-doping. This is rather surprising since at low GB angles, part of the benefit of Ca-doping is to reduce the strain fields around the dislocations. This effect being absent with IL gating one might have expected a lower effectiveness of our technique compared to Ca-doping at comparable average doping capability.

Part of the answer possibly resides in the fact that, at our underdoped GB, λ_D is probably larger. Hence a comparable variation of the local carrier density might be more effective in reducing λ_D in our case than for optimally doped GBs. This could then compensate the absence of doping induced strain reduction with gating. On the other hand, it has been pointed by Gurevich and Pashitskii⁹ that, in the underdoped state, the effect of strain is inducing very large T_c variations at GBs. Hence, it would be very interesting to investigate the effect of Ca-doping at underdoped low angle GBs. This would allow a direct comparison with our strain-tuning-free technic and possibly a quantification of the importance of strain release in the improvement of the transport properties of cuprate GBs obtained by Ca-doping.

In summary, we have presented evidences for the strong tuning of the transport properties of GBs in underdoped YBCO films using IL gating. By studying the evolution of B_{irr} in samples with different initial doping levels, we have shown that this tuning modifies the transport in the presence of a magnetic field too. Further analyses of our data have shown that assuming the theory developed in¹² for low-angle grain boundaries to apply, we can spotlight a large evolution of the local depairing density at the GB. Finally, we have discussed our data in the perspective of the very successful Ca-doping of GBs. Our results indicate that the carrier modulation induced in this study is of the same order of magnitude than the overdoping obtained by substituting Y^{3+} by Ca^{2+} . We believe that, thanks to its ability to improve the carrier density without modifying the strain level at the GB, IL gating offers a new opportunity to investigate the transport properties of cuprate GBs which might ultimately lead to the tailoring of new dopants.

Methods

Growth. 5, 7 and 10 unit cells (uc) thick YBCO films were deposited by pulsed laser interval deposition on (001)-oriented, [001]-tilt ($\theta = 8^\circ$) SrTiO₃ bi-crystals (MTI corp.). A non-superconducting PrBa₂Cu₃O_{7-x} (PBCO) layer was used as a buffer in-between the YBCO and the substrate. Its thickness was 20, 10 and 10uc respectively. Compared to our previous publication¹¹, were more details on the fabrication process can be found, slight optimizations of the growth conditions were made. Here, the growth temperature of the PBCO and YBCO layers is 820 °C and 830 °C respectively, 0.18 mbar of pure O₂ are used during the deposition process and the target-substrate distance is 49 mm. As terminated SrTiO₃ bi-crystals are not commercially available, TiO₂ termination was achieved *in-house* following the buffered-HF + high temperature annealing road^{38,39}.

Characterization. Standard photolithography techniques were used to align a 10 μm wide, 150 μm long channel with the GB (see Fig. 1). Alignment was made manually, using an optical microscope. In general the GB was crossing the channel at mid-distance between the two central voltage taps ($\pm 10\%$ of accuracy). The measurements were performed in a cryostat equipped with a unipolar 19 magnet with no particular magnetic shield for the sample. Hence, we use the notation “sf*” to indicate the presence of a remanent field. The ionic liquid we used is DEME-TFSI (CAS No. 464927-84-2), which is a quite standard choice to perform IL gating experiments. Due to its glassy state below ~180 K, gate voltage was modified only at 240 k. V_g was raised gradually by increments of 10–50 mV. After a given setpoint was reached, the sample was kept during several hours (~4 to 10 h) at the same temperature and gate voltage. This relaxation step is necessary as the doping of the system proceeds in rather slow manner. More details on the use of the ionic liquid and on the relaxation process can be found in¹¹.

Data Availability Statement

Data are available upon request.

References

- Hilgenkamp, H. & Mannhart, J. Grain boundaries in high- T_c superconductors. *Rev. Mod. Phys.* **74**, 485 (2002).
- Gross, R., Chaudhari, P., Kawasaki, M., Ketchen, M. B. & Gupta, A. Low noise YBa₂Cu₃O_{7-x} grain boundary junction dc SQUIDS. *Appl. Phys. Lett.* **57**, 727 (1990).
- Faley, M. I. *et al.* High- T_c SQUID biomagnetometers. *Supercond. Sci. Technol.* **30**, 083001 (2017).

4. Iijima, Y., Tanabe, N., Kohno, O. & Ikeno, Y. In plane aligned YBa₂Cu₃O_{7-x} thin films deposited on polycrystalline metallic substrates. *Appl. Phys. Lett.* **60**, 769 (1992).
5. Obradors, X. & Puig, T. Coated conductors for power applications: materials challenges. *Supercond. Sci. Technol.* **27**, 044003 (2014).
6. Superpower, inc. reports world records, progress to doe <http://www.superpower-inc.com/content/superpower-inc-reports-world-records-progress-doe> (2009).
7. Goyal, A. *et al.* Conductors with controlled grain boundaries: An approach to the next generation, high temperature superconducting wire. *J. Mater. Res.* **12**, 2924 (1997).
8. Groves, J. *et al.* Texture development in IBAD MgO films as a function of deposition thickness and rate. *IEEE Transactions on Applied Supercond.* **11**, 2822 (2001).
9. Gurevich, A. & Pashitskii, E. A. Current transport through low-angle grain boundaries in high-temperature superconductors. *Phys. Rev. B* **57**, 13878 (1998).
10. Gurevich, A. Nonlinear viscous motion of vortices in Josephson contacts. *Phys. Rev. B* **48**, 12857–12865 (1993).
11. Fete, A., Rossi, L., Augieri, A. & Senatore, C. Ionic liquid gating of ultra-thin YBa₂Cu₃O_{7-x} films. *Appl. Phys. Lett.* **109**, 192601 (2016).
12. Gurevich, A. Nonlinear dynamics of vortices in easy flow channels along grain boundaries in superconductors. *Phys. Rev. B* **65**, 214531 (2002).
13. Schmehl, A. *et al.* Doping-induced enhancement of the critical currents of grain boundaries in YBa₂Cu₃O_{7-δ}. *Europhys. Lett.* **47**, 110 (1999).
14. Dhoot, A. S. *et al.* Increased T_c in Electrolyte-Gated Cuprates. *Adv. Mater.* **22**, 2529 (2010).
15. Bollinger, A. T. *et al.* Superconductor-insulator transition in La_{2-x}Sr_xCuO₄ at the pair quantum resistance. *Nat.* **472**, 458 (2011).
16. Nojima, T. *et al.* Hole reduction and electron accumulation in YBa₂Cu₃O_y thin films using an electrochemical technique: Evidence for an n-type metallic state. *Phys. Rev. B* **84**, 020502 (2011).
17. Leng, X., Garcia-Barriocanal, J., Bose, S., Lee, Y. & Goldman, A. M. Electrostatic control of the evolution from a superconducting phase to an insulating phase in ultrathin YBa₂Cu₃O_{7-x} films. *Phys. Rev. Lett.* **107**, 6–9 (2011).
18. Leng, X. *et al.* Indications of an electronic phase transition in two-dimensional superconducting YBa₂Cu₃O_{7-x} thin films induced by electrostatic doping. *Phys. Rev. Lett.* **108**, 1 (2012).
19. Salluzzo, M. *et al.* Thickness effect on the structure and superconductivity of Nd_{1.2}Ba_{1.8}Cu₃O_z epitaxial film. *Phys. Rev. B* **72**, 134521 (2005).
20. Daniels, G. A., Gurevich, A. & Larbalestier, D. C. Improved strong magnetic field performance of low angle grain boundaries of calcium and oxygen overdoped YBa₂Cu₃O_x. *Appl. Phys. Lett.* **77**, 3251 (2000).
21. Gurevich, A. Nonlocal Josephson electrostatics and pinning in superconductors. *Phys. Rev. B* **46**, 3187–3190 (1992).
22. Gurevich, A. Nonlinear dynamics of vortices in high-J_c Josephson contacts. *Phys. C* **243**, 191–196 (1995).
23. Carapella, G., Sabatino, P., Barone, C., Pagano, S. & Gombos, M. Current driven transition from Abrikosov-Josephson to Josephson-like vortex in mesoscopic lateral S/S'/S superconducting weak links. *Sci. Reports* **6**, 35694 (2016).
24. Gurevich, A. *et al.* Flux Flow of Abrikosov-Josephson Vortices along Grain Boundaries in High-Temperature Superconductors. *Phys. Rev. Lett.* **88**, 097001 (2002).
25. Hogg, M. J., Kahlmann, F., Tarte, E. J., Barber, Z. H. & Evetts, J. E. Vortex channeling and the voltage-current characteristics of YBa₂Cu₃O₇ low-angle grain boundaries. *Appl. Phys. Lett.* **78**, 1433 (2001).
26. Gurevich, A. & Cooley, L. D. Anisotropic flux pinning in a network of planar defects. *Phys. Rev. B* **50**, 13563 (1994).
27. Sarnelli, E. & Testa, G. Transport properties of high-temperature grain boundary Josephson junctions. *Phys. C: Supercond.* **371**, 10 (2002).
28. Blatter, G., Feigel'man, M. V., Geshkenbein, V. B., Larkin, A. I. & Vinokur, V. M. Vortices in high-temperature superconductors. *Rev. Mod. Phys.* **66**, 1125 (1994).
29. Kupriyanov, M. Y. & Lukichev, V. F. Temperature dependence of the pair-breaking current density in superconductors. *Fiz. Nizk. Temp.* **6**, 445 (1980).
30. Grissonnanche, G. *et al.* Direct measurement of the upper critical field in cuprate superconductors. *Nat. Commun.* **5** (2014).
31. Zuev, Y., Seog Kim, M. & Lemberger, T. R. Correlation between Superfluid Density and TC of Underdoped YBa₂Cu₃O_x Near the Superconductor-Insulator Transition. *Phys. Rev. Lett.* **95**, 137002 (2005).
32. Guth, K., Krebs, H. U., Freyhardt, H. C. & Jooss, C. Modification of transport properties in low-angle grain boundaries via calcium doping of YBa₂Cu₃O_δ thin films. *Phys. Rev. B* **64**, 140508 (2001).
33. Klie, R. F. *et al.* Enhanced current transport at grain boundaries in high-T_c superconductors. *Nat.* **435**, 475 (2005).
34. Song, X., Daniels, G., Feldmann, D. M., Gurevich, A. & Larbalestier, D. Electromagnetic, atomic structure and chemistry changes induced by Ca-doping of low-angle YBa₂Cu₃O_{7-δ} grain boundaries. *Nat. Mater.* **4**, 470 (2005).
35. Li, P., Abramov, D., Polyanskii, A., Kametani, F. & Larbalestier, D. Study of grain boundary transparency in (Yb_{1-x}Ca_x)Ba₂Cu₃O₂ bicrystal thin films over a wide temperature, field, and field orientation range. *Phys. Rev. B* **91**, 104504 (2015).
36. Uesugi, E., Goto, H., Eguchi, R., Fujiwara, A. & Kubozono, Y. Electric double-layer capacitance between an ionic liquid and few-layer graphene. *Sci. Reports* **3**, 1595 (2013).
37. Presland, M., Tallon, J., Buckley, R., Liu, R. & Flower, N. General trends in oxygen stoichiometry effects on T_c in Bi and Tl superconductors. *Phys. C: Supercond.* **176**, 95 (1991).
38. Kawasaki, M. *et al.* Atomic Control of the SrTiO₃ Crystal. *Surface. Sci.* **266**, 1540 (1994).
39. Koster, G., Kropman, B. L., Rijnders, G. J. H. M., Blank, D. H. A. & Rogalla, H. Quasi-ideal strontium titanate crystal surfaces through formation of strontium hydroxide. *Appl. Phys. Lett.* **73**, 2920–2922 (1998).

Acknowledgements

The authors would like to thank D. Zurmuehle and X. Ravinet for their technical assistance as well as D. Stornaiuolo and C. Berthod for stimulating discussions. Financial support was provided by the SNSF (Grant No. PP00P2_144673).

Author Contributions

A.F. performed the sample growth, device fabrication, and electrical measurements. A.F. analyzed the data and wrote the manuscript. C.S. directed the research and contributed to manuscript preparation.

Additional Information

Supplementary information accompanies this paper at <https://doi.org/10.1038/s41598-018-36166-w>.

Competing Interests: The authors declare no competing interests.

Publisher's note: Springer Nature remains neutral with regard to jurisdictional claims in published maps and institutional affiliations.



Open Access This article is licensed under a Creative Commons Attribution 4.0 International License, which permits use, sharing, adaptation, distribution and reproduction in any medium or format, as long as you give appropriate credit to the original author(s) and the source, provide a link to the Creative Commons license, and indicate if changes were made. The images or other third party material in this article are included in the article's Creative Commons license, unless indicated otherwise in a credit line to the material. If material is not included in the article's Creative Commons license and your intended use is not permitted by statutory regulation or exceeds the permitted use, you will need to obtain permission directly from the copyright holder. To view a copy of this license, visit <http://creativecommons.org/licenses/by/4.0/>.

© The Author(s) 2018